

# Identification of Novel Bioactive Phytochemicals from *Solanum torvum* as AKT1 Regulator against Breast Cancer: An *In-Silico* Approach

Kaliraj Chandran <sup>1</sup> , Azar Zochedh <sup>1</sup> , Asath Bahadur Sultan <sup>2,\*</sup> , Thandavarayan Kathiresan <sup>1,\*</sup> 

<sup>1</sup> Department of Biotechnology, Kalasalingam Academy of Research and Education, Krishnankoil, Tamil Nadu, India

<sup>2</sup> Condensed Matter Physics Laboratory, Department of Physics, International Research Center, Kalasalingam Academy of Research and Education, Krishnankoil, Tamil Nadu, India

\* Correspondence: s.asathbahadur@gmail.com (A.B.S.); t.kathiresan@klu.ac.in (T.K.);

Scopus Author ID 57215079667

Received: 26.04.2023; Accepted: 28.05.2023; Published: 28.09.2024

**Abstract:** *Solanum torvum* L. is a wild medicinal plant frequently found in the Indian subcontinent. AKT1 is an excellent anticancer target against breast cancer, as cell invasion and motility are reduced by AKT1 inhibition despite the possibility that AKT1 activation may promote cell growth. In this study, the ten bioactive phytochemicals from *S. torvum* were docked against the breast cancer-associated target protein AKT1 and compared with the known drug tamoxifen. Among the ten bioactive compounds, three phytochemicals, Spirostane-3,6-dione, chlorogenin, and beta-sitosterol-d-glucoside, exhibited higher binding ability compared to standard Tamoxifen with docking scores of -17.4, -12.2 and -11.5 Kcal/mol. These top-hit bioactive compounds were further investigated for their structural stability and reactivity based on frontier molecular orbitals, and the electronic spectrum reveals the excitation states through density functional theory at B3LYP/6-311 G level. The electronic transitions observed were  $\pi \rightarrow \pi^*$  and  $\sigma \rightarrow \sigma^*$ . The drug-likeness characteristics of the top-hit bioactive compounds were assessed based on absorption, distribution, metabolism, excretion, toxicity, and physicochemical parameters. This *in silico* research will promote the use of *S. torvum* in conventional therapy and the initiation of an *in vitro model* to develop new medicines to treat breast cancer.

**Keywords:** *Solanum torvum*; breast cancer, AKT1; molecular docking; DFT; ADMET.

© 2024 by the authors. This article is an open-access article distributed under the terms and conditions of the Creative Commons Attribution (CC BY) license (<https://creativecommons.org/licenses/by/4.0/>).

## 1. Introduction

*Solanum torvum* L. is a wild medicinal plant commonly present in the Indian subcontinent regions, and it is commonly called a Turkey berry. *S. torvum* was widely used as a traditional food item in South India [1]. In Tamil literature, *S. torvum* is known as 'Sundai' and was used as a traditional medication to treat acute bronchitis [2]. Both *S. torvum* plant's leaves and fruits were utilized as edible vegetables, either cooked or raw. The extracted phenolic compounds from *S. torvum* show antioxidant activity and also fight against mycobacterium infections like tuberculosis and leprosy [3, 4]. It also possesses a higher potential for cancer-inhibitory properties [5]. Breast cancer is a type of malignancy that occurs in the mammalian cells. Most often, breast cancer develops in one of the two sectors of the breast termed lobules or ducts. Cancer may form in the breast's fat tissues, known as adipose tissue, as well as in the connective tissue. Uncontrolled cancer cells in the breast typically infect other normal tissues and have a high risk of moving toward the lymph nodes beneath the arms

[6]. Akt/Protein Kinase B acts as an emerging breast cancer inhibitor protein. Among the three isoforms of the Akt family, Akt1 was performed as an excellent anticancer target against breast cancer cells by regulating apoptosis and proliferation. The activation of the Akt1 may lead to cell proliferation, but the cell invasion and motility will be suppressed by inhibition of Akt1 [7]. The most typically disrupted pathway in various cancers is the PI3K/AKT pathway [8]. AKT is a serine-threonine kinase that is involved in various downstream signaling pathways that control mechanisms such as cell metabolism, cell division, cell differentiation, cell proliferation, and apoptosis [9]. Each of them is related to many cancers, including ovarian, breast cancer, colon cancer, stomach cancer, hormone-insensitive breast cancer, and prostate cancer [10, 11]. Akt1 is typically up-regulated in human cancers, and it has been reported to increase cell proliferation while inhibiting programmed cell death. As a result, inhibiting Akt1 activity has been identified as an appealing therapeutic target [12]. Mammary epithelial tumor cells (MEC) lacking Akt1 appeared tiny and less proliferative, with lower levels of cyclin D1 and p27KIP1 [13]. The most common cause of breast cancer death is metastasis. PtdIns (3, 4, 5) P3 generated by PI3K activates AKT, which actively encourages the proliferation of cancer cells and is responsible for regulating migration. Until today, no inositol polyphosphate 5-phosphatases have been found as breast cancer tumor suppressors that inhibit PI3K/AKT signaling [14]. Akt1 suppresses the migration of breast cancer cells by boosting the breakdown of the transcription factor NFAT (nuclear factor of activated T cells) [15]. The regulation of extracellular signal-regulated kinase/mitogen-activated protein kinase (ERK/MAPK) was also performed by Akt1 [16]. Genetic mutations within the AKT pleckstrin homology domain have been found to disrupt localization, cause loss of sensitivity to phosphatidylinositols, and significantly affect AKT functional behavior [17].

In the current investigation, the bioactive constituents from the *Solanum torvum* were screened and analyzed for binding ability against the breast cancer-associated target protein through molecular docking studies. Then the top hit phytochemical was analyzed for its structural stability and reactivity through density function theory in B3LYP/6-311 G basis level based on HOMO, LUMO, and band energy gap. The electronic spectrum reveals the excitation energy, orbital contribution, and their assignments. Further, the drug-likeness feature of the top-hit bioactive compounds from the *S. torvum* was evaluated through physicochemical, absorption, distribution, metabolism, excretion, and toxicity parameters. These *in silico* findings will pave the way for *in vitro* and *in vivo* investigation of bioactive phytochemicals from *S. torvum* against breast cancer.

## 2. Materials and Methods

### 2.1. Graph theory network analysis.

The functional partners of the protein AKT1 in Homo sapiens were selected in order to determine the important proteins. The Cytoscape 3.9.1 software and STRING (functional protein association network) were used to create the graph theoretical network analysis. The homo sapiens group used the STRING web server to look for the target protein AKT1. The CSV file that Cytoscape requested was then exported from the results that were created. After inserting the exported data into Cytoscape's graphical window, the network's total number of edges, nodes, and edges were examined [18].

## 2.2. Protein retrieval and preparation.

The RCSB Protein Data Bank (PDB: <http://www.rcsb.org/pdb>) was used to get the crystal structure of AKT1 at 2.70 Å resolution [19]. Using the BIOVIA Discovery Studio 2021 software, obtained protein structures were further processed by eliminating water molecules, hetatms, and existing ligand molecules.

## 2.3. Bioactive compounds retrieval.

We identified nearly ten bioactive phytochemicals in *S. torvum* using Dr. Duke's Phytochemical and Ethnobotanical database and IMPAAT database [20,21]. The Three-Dimensional structures in ".sdf" format of the bioactive phytochemicals present in *S. torvum* were acquired from the PubChem database (<https://pubchem.ncbi.nlm.nih.gov/>) [22].

## 2.4. Active site identification.

An active site, also known as a binding site, is a specific location on a protein that permits the ligand to attach and perform a reaction. The CASTp (Computed Atlas of Surface Topography of Proteins) online web tool (<http://sts.bioe.uic.edu/castp/index.html?3o96>) was utilized to recognize and confirm the active site of the targeted receptor protein AKT1 (PDB ID: 3O96) [23]. This tool assists us in recognizing all the active parts and the target protein's vital information. Uploading the finalized target structure uses a PDB or Job ID. Several pockets emerged during the analysis, and the perfect pocket was identified by utilizing the overall area and volume of active regions contained inside the target structure.

## 2.5. Molecular docking studies.

In the novel drug design process, a computational method known as molecular docking simulation is first used. The molecular docking was achieved by using freely accessible software known as PyRx 0.8. The biologically active phytochemicals from *S. torvum* were used to dock against the breast cancer-associated target protein AKT1 (PDB ID: 3O96). The retrieved ligand molecules of the *S. torvum*, along with the common drug used to treat breast cancer (Tamoxifen), were imported in the graphical window. After that, all the ligand structures were minimized, and the ligands were converted into the ".pdbqt" format. The predicted active site of the macromolecule was covered with a grid box, and then the molecular docking simulation was performed. All the bioactive compounds were picked and analyzed through docking simulation. The prediction of bond interaction types, number of hydrogen bonds, and bond distances were examined, and the interaction between the protein and ligands was visualized as images through 2D and 3D images using Discovery Studio.

## 2.6. Physicochemical properties and bioactivity scores.

The bioactivity score and physicochemical characteristics of the lead phytochemical from *S. torvum* were predicted using the SwissADME (<http://www.swissadme.ch/>) and Molinspiration (<https://www.molinspiration.com/>) servers. To calculate the bioactivity score and physicochemical characteristics of the lead compound, the SMILES of the bioactive lead compound were obtained from the PubChem database (<https://pubchem.ncbi.nlm.nih.gov/>) and examined using the Molinspiration and SWISS ADME servers. Molecular weight, log P, hydrogen bond donors and acceptors, total polar surface area, and the number of rotatable

bonds were all analyzed using SwissADME. Bioactivity values such as protease inhibitor, nuclear receptor ligand, kinase inhibitor, and bioavailability scores were created via the Molinspiration server of Molinspiration Cheminformatics [24, 25].

### 2.7. Pharmacokinetic prediction.

The absorption, distribution, metabolism, excretion, and toxicity model analyses of the bioactive lead chemical from *S. torvum* were performed using the online program pkCSM (<http://biosig.unime.lb.edu.au/pkcsm/prediction>). The canonical SMILES used in this study were obtained from the PubChem online database, which can be accessed at <https://pubchem.ncbi.nlm.nih.gov>. The pkCSM server was used to get toxicity evaluations of the bioactive phytochemicals, with a focus on AMES toxicity and hepatotoxicity. AMES toxicity and hepatotoxicity are included among the toxicity profiles for phytochemical absorption (Caco2 permeability, intestinal permeability, and skin permeability), distribution (VD<sub>ss</sub>, BBB, and CNS permeability), metabolism (effect on cytochromes P450 and P-gp substrate), excretion (total clearance and renal OCT2 substrate), and toxicity. The profiles of *S. torvum* phytochemicals were gathered using the pkCSM web server [26].

### 2.8. Quantum chemical calculations.

The quantum chemical calculation was performed through the Gaussian 09W program in the B3LYP function with the basis set of 6-311G [27]. The 3-dimensional structure of the top hit compound was given as input in the Gaussian software. The top-hit compounds' chemical reactivity and their structural stability were assessed through molecular orbitals. The frontier molecular orbitals were calculated based on the energy difference between LUMO and HOMO. These Gaussian results were visualized through the GaussView 5 tool [28]. The electronic states in the top hit compound were evaluated through theoretical UV-visible spectrum performed through TD-DFT function with the same basis set [29]. The type of transition, the contribution of each transition, and its assignments were assessed.

## 3. Results and Discussion

### 3.1. Graph theory network analysis.

The STRING and Cytoscape programs were utilized to generate a graph representing the network of the AKT1 pathway [30]. Figure 1 in the current study endeavor displayed a variety of functional partner protein entities and their relationships. According to centrality characteristics such as betweenness, eccentricity, proximity, degree, stress, and radiality, the network consists of 11 nodes and 40 edges. The functional partners were assessed to be PH domain leucine-rich repeat-containing protein phosphatase 1 (PHLPP1), DCC-interacting protein 13-alpha (APPL1), Nitric-oxide synthase (NOS3), Heat shock protein HSP 90-alpha (HSP90AA1), Serine/threonine-protein kinase mTOR (MTOR), Forkhead box protein O3 (FOXO3), E3 ubiquitin-protein ligase Mdm2 (MDM2), Histone acetyltransferase p300 (EP300), Phosphatidylinositol 4,5-bisphosphate 3-kinase catalytic subunit alpha isoform (PIK3CA) and Rapamycin-insensitive companion of mTOR (RICTOR).

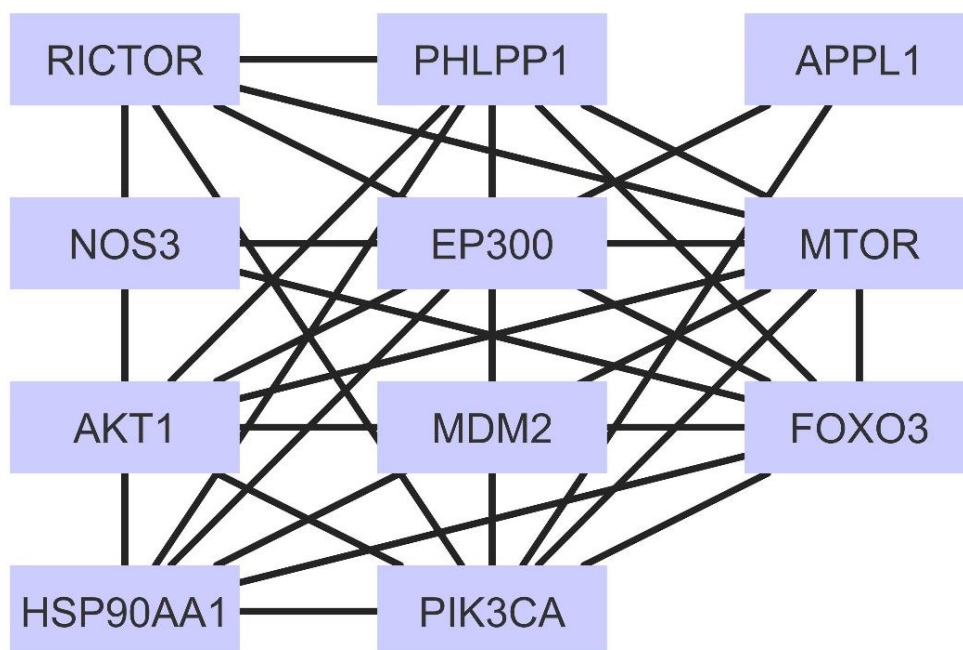


**Figure 1.** Constructed a network of functional partners of AKT1 in breast cancer.

The statistics of the network for AKT1 exhibited eleven nodes, forty edges, an average number of 7.273 neighbors, two network diameters, one network radius, 1.273 characteristic pathlength, a clustering coefficient of 0.874, a network density of 0.727, and network heterogeneity and centralization of 0.305 and 0.333, respectively. The centrality measures of the AKT1 network are tabulated in Table 1. The greater values of all the centrality measures were detected on AKT1, and the values of degree, betweenness, closeness, radiality, and stress were 10, 0.131852, 1, 1, and 30, respectively. Depending on the outcome of the centrality measure and its threshold values, the protein AKT1 was recognized as a potential target for breast cancer. It can be utilized as a target protein in the molecular docking simulation.

**Table 1.** The results of the AKT1 network analysis's threshold parameter standards.

Centrality measures	Degree	Betweenness	Closeness	Radiality	Stress
AKT1	10	0.131852	1	1	30
MDM2	7	0.003704	0.769231	0.97	2
PHLPP1	7	0.003704	0.769231	0.97	2
EP300	7	0.008889	0.769231	0.97	4
PIK3CA	9	0.08963	0.909091	0.99	20
APPL1	2	0	0.555556	0.92	0
RICTOR	6	0	0.714286	0.96	0
NOS3	5	0	0.666667	0.95	0
HSP90AA1	9	0.031852	0.909091	0.99	14
MTOR	9	0.031852	0.909091	0.99	14
FOXO3	9	0.031852	0.909091	0.99	14

### 3.2. Active site prediction.

Active regions of the target protein AKT1 were predicted through the CASTp v.3.0 algorithm [31]. As investigated by the CASTp, an AKT1 has 40 active pockets. The prominent ideal active region should have a larger surface area and volume than the other active regions. Even though the active site areas of AKT1 were established, the CASTp assisted in covering additional possible pockets in the active regions of the aforementioned target protein through their optimum scores. CASTp findings reveal the optimal pockets and chains in the target protein's active areas. The residues found in chain A of the target protein AKT1 were analyzed

to be in the active areas. Among the predicted active pockets of AKT1, an ideal pocket containing a larger surface area of 1665.060 Å<sup>2</sup> and volume of 1365.991 Å<sup>3</sup> was picked as an active region (Figure 2), which has the following residues of A\_14, A\_15, A\_16, A\_17, A\_18, A\_20, A\_25, A\_27, A\_28, A\_30, A\_34, A\_36, A\_37, A\_38, A\_39, A\_40, A\_42, A\_43, A\_44, A\_45, A\_49, A\_50, A\_51, A\_52, A\_53, A\_54, A\_55, A\_56, A\_58, A\_59, A\_77, A\_78, A\_79, A\_80, A\_81, A\_82, A\_83, A\_84, A\_85, A\_86, A\_87, A\_161, A\_199, A\_201, A\_202, A\_205, A\_206, A\_207, A\_210, A\_211, A\_212, A\_213, A\_216, A\_217, A\_218, A\_223, A\_224, A\_225, A\_227, A\_263, A\_264, A\_268, A\_270, A\_271, A\_272, A\_273, A\_274, A\_276, A\_279, A\_290, A\_291, A\_292, A\_293, A\_294, A\_296, A\_297, A\_298, A\_316, A\_319, A\_320, A\_323, A\_324, A\_325, A\_326, A\_327, A\_328, A\_329, A\_388, A\_389, A\_393, A\_394, A\_395, A\_396 and A\_398. These residues were selected and utilized for selective docking, allowing the interaction profile to be examined. During the molecular docking method, these active site areas of the target protein AKT1 were used. Using these active site areas, a grid box was created in the target protein to allow the ligand to bind. Docking in active areas may increase binding affinity and improve docking scores for ligands.

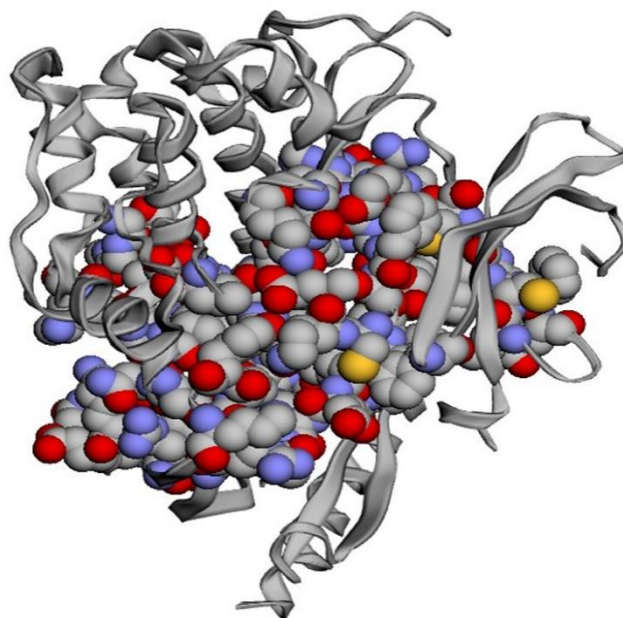


**Figure 2.** Identified active site regions of AKT1 protein through the CASTp online server.

### 3.3. Molecular docking analysis.

A molecular docking investigation was performed to analyze the binding ability of the bioactive phytochemicals present in *S. torvum* at the receptor region of the target protein. For the molecular docking simulation against the breast cancer-associated protein AKT1 (PDB:ID: 3O96), the *S. torvum*'s ten bioactive phytochemicals were picked. The molecular docking simulations were performed using PyRx. The open web server CASTp was used to determine the expected active areas of receptor proteins. The grid box was built using the anticipated active areas of the targeted receptor protein, and docking was then performed [32]. The common anticancer medicine Tamoxifen was utilized to compare the *S. torvum* bioactive phytochemicals' capacity for anticancer action. The docking score of bioactive compounds and the standard Tamoxifen, was tabulated in Table 2. The binding affinity of the common Tamoxifen, which was docked with AKT1, is -10.9 kcal/mol. Spirostane-3,6-dione, which has a score of -17.4 kcal/mol, has the greatest binding affinity of all the bioactive phytocompounds in *S. torvum*. Compared to the usual drug tamoxifen, the lead bioactive spirostane-3,6-dione

exhibits a strong affinity for binding. The bioactive phytochemicals of *S. torvum* had docking findings that vary from -5.2 to -17.4 kcal/mol. With a score of -5.2, niacin has the lowest binding affinity for AKT1. With an AKT1 receptor protein, chlorogenin and  $\beta$ -Sitosterol-d-glucoside exhibit greater binding affinities of -12.2 and -11.5 kcal/mol, respectively. Torvogenin and riboflavin have binding affinities of -10.0 and -9.7 kcal/mol, respectively, while  $\beta$ -Carotene, retinol, sisalagenone, and ascorbic acid have binding affinities of -9.3, -9.2, and -9.1 kcal/mol, respectively. The lead phytochemical identified by the outcomes of the molecular docking simulation was spirostane-3,6-dione, which may prevent metastatic breast cancer by regulating or inhibiting AKT1.

**Table 2.** Docking scores of bioactive phytochemicals from *S. torvum* and Tamoxifen against target protein AKT1.

S. No	PubChem CID	Phytochemicals	AKT1 (PDB ID: 3O96)
1	54670067	Ascorbic Acid	-5.8
2	5280489	Beta-Carotene	-9.3
3	12309060	Beta-Sitosterol-d-glucoside	-11.5
4	12303065	Chlorogenin	-12.2
5	938	Niacin	-5.2
6	445354	Retinol	-9.2
7	493570	Riboflavin	-9.7
8	52321340	Sisalagenone	-9.1
9	13889197	Spirostane-3,6-dione	-17.4
10	11554175	Torvogenin	-10.0
11	2733526	Tamoxifen (Standard drug)	-10.9

#### 3.4. Analysis of protein-ligand interactions.

Using BIOVIA Discovery Studio 2021, the interacting amino acids, different bond interactions, and bond lengths were identified. Figures 2-4 depict the amino acid interactions between lead phytochemicals and the AKT1 receptor protein linked to breast cancer. The top binding Spirostane-3,6-dione with AKT1 formed four (4) conventional hydrogen bonds with amino residue ASN53, SER205, and LYS268 (2) at a bond distance (Å) of 2.55187, 2.3054, 2.62441, and 2.7624, respectively and also established two (2) attractive charge and one (1) pi-cation electrostatic interactions with amino residue ASP292 (2), and TRP (80) at bond distances of (Å) 5.48754, 4.66229, and 4.09162, respectively and also produced five (5) alkyl and three (3) pi-alkyl hydrophobic interactions with amino residue LYS268, VAL270, LEU264, LEU210, LEU264, and TRP80 (3) at bond distances (Å) of 4.86665, 4.25069, 4.94268, 3.93443, 5.11825, 4.4259, 4.65369, and 4.57981, respectively. The second top binding bioactive chlorogenin with AKT1 produced two (2) pi-sigma, seven (7) alkyl, and five (5) pi-alkyl hydrophobic interactions with amino residue TRP80 (2), LYS268, VAL270 (2), LEU264, LYS268, VAL270, ILE84, TRP80 (4) and TYR272 at bond distances(Å) of 2.40175, 2.3442, 4.30844, 5.26479, 4.20238, 4.02151, 4.61533, 3.35262, 5.00536, 5.08586, 4.31261, 4.93783, 3.83414, and 4.42527, respectively. The third top binding phytocompound  $\beta$ -Sitosterol-d-glucoside with AKT1 formed three (3) conventional hydrogen bond and two (2) carbon-hydrogen bond interactions with amino residue ARG273, TYR326, GLU85 (2), and GLU17 at bond distances (Å) 2.79825, 2.68445, 1.80845, 3.01716, and 2.49427, respectively and also established six (6) alkyl and five (5) pi-alkyl with amino residue ILE84, ARG273, VAL270, LEU210, LEU264, LEU210, and TRP80 (5) at bond distances (Å) of 4.96194, 4.11975, 3.84754, 3.75729, 5.24239, 4.90162, 5.14097, 4.68764, 4.41563, 5.15576, and 4.69054, respectively. The phytocompound Torvogenin with AKT1 formed two (2) conventional hydrogen bond and three (3) carbon-hydrogen bond interactions with amino

residue VAL271, TYR272 (2), and GLN79 (2) at bond distances (Å) of 2.29346, 2.75639, 2.55534, 2.25951, and 2.35456, respectively and also produced five (5) alkyl and one (1) pi-alkyl with amino residue ILE84, VAL270, ARG273, ILE84, VAL270, and TYR272 at bond distances (Å) of 5.42311, 5.05321, 5.15729, 4.33407, 4.44611 and 4.03459, respectively. The phytochemical Riboflavin with AKT1 formed two (2) conventional hydrogen bond and three (3) carbon-hydrogen bond interactions with amino residue THR82, ASP292, THR82 (2), AND ASP292 at bond distances (Å) of 2.05829, 2.95079, 2.58767, 2.84764, and 2.67134, respectively and also produced one (1) pi-anion electrostatic interaction with amino residue ASP292 at the bond distance of 4.8322 Å, respectively and also established five (5) pi-pi stacked, three (3) alkyl, and six (6) pi-alkyl hydrophobic interactions with amino residue TRP80 (5), LYS268, VAL270, LYS268, TRP80, LEU264, LEU210, LEU264, LYS268, and VAL270 at bond distances (Å) of 3.83142, 4.96346, 4.02244, 4.67779, 3.98953, 4.50086, 4.05558, 3.65736, 4.2127, 4.89974, 4.33321, 5.17513, 4.36454 and 5.13002, respectively. The phytochemical  $\beta$ -carotene formed one (1) pi-sigma, six (6) alkyl, and two (2) pi-alkyl with amino residue TRP80, VAL270, ILE84, CYS296, LEU264, VAL270 (2), and TRP80 at bond distances (Å) of 2.2777, 4.19184, 5.11404, 4.63331, 3.8557, 4.4708, 4.1562, 4.14815, and 5.19832, respectively. The phytochemical Retinol with AKT1 formed three (3) conventional hydrogen bond interactions with amino residue GLN79, ASN53, and SER56 at bond distances (Å) of 2.73981, 2.36437, and 2.34205, respectively, and also established ten (10) alkyl, and seven (7) pi-alkyl with amino residue LEU210, LEU264, LYS268, VAL270 (2), LYS268, VAL270, LEU264, TRP80 (7) at bond distances (Å) of 4.94054, 4.44861, 5.34082, 4.41175, 5.46119, 3.69729, 4.656, 4.13126, 4.44336, 5.46213, 4.06155, 4.9165, 4.65417, 4.1125, 4.53407, 5.00159, and 4.33845, respectively. The phytochemical Sisalagenone with AKT1 formed five (5) conventional hydrogen bond and three (3) carbon-hydrogen bond interactions with amino residue TYR272, PHE293, GLY294, ASP292, ASP274, ASP292, SER205, and THR211 at bond distances (Å) of 2.27804, 2.27005, 2.48447, 2.17177, 2.71349, 2.17032, 3.06597, and 2.98514, respectively and also established one (1) halogen (fluorine) interaction and one (1) pi-anion electrostatic interaction with amino residue ASP292 (2) at bond distances (Å) of 3.69935 and 4.87003, respectively and also produced two (2) pi-pi stacked and four (4) pi-alkyl with TRP80 (4), LEU210, and LEU264 at bond distances (Å) of 4.11326, 5.24999, 4.68817, 4.85664, 4.85664, 4.9863, and 5.22029, respectively. The phytochemical Ascorbic acid with AKT1 formed six (6) conventional hydrogen bond and two (2) carbon-hydrogen bond interactions with amino residue ASN54, THR81, GLN79, TYR272, VAL271, TYR272, THR82, and ASP292 at bond distances (Å) of 2.69756, 2.19932, 2.13998, 2.60718, 2.07968, 2.83374, 2.9567, and 2.46251, respectively. The Phytochemical Niacin with AKT1 formed two (2) conventional hydrogen bonds and two (2) carbon-hydrogen bond interactions with amino residue TRP80, ILE290, THR211, and THR291 at bond distances (Å) of 2.81434, 2.07745, 2.15597, and 3.01555, respectively and also produced two (2) alkyl and one (1) pi-alkyl hydrophobic interactions with amino residue LEU210, LEU264, and TYR272, respectively. The molecular docking simulation shows the top-hit compound's capacity to bind to the target protein at its active receptor regions by the kind of bond interaction, bond length, and donor and acceptor regions of the hydrogen bond [33-36]. Effective binding ability, robust hydrogen bond interactions, and other bond interactions with the amino acids located at the active sites of the target protein are an advantage for spirostane-3,6-dione, chlorogenin, and  $\beta$ -Sitosterol-d-glucoside to be successful therapeutic agents for the treatment of breast cancer.

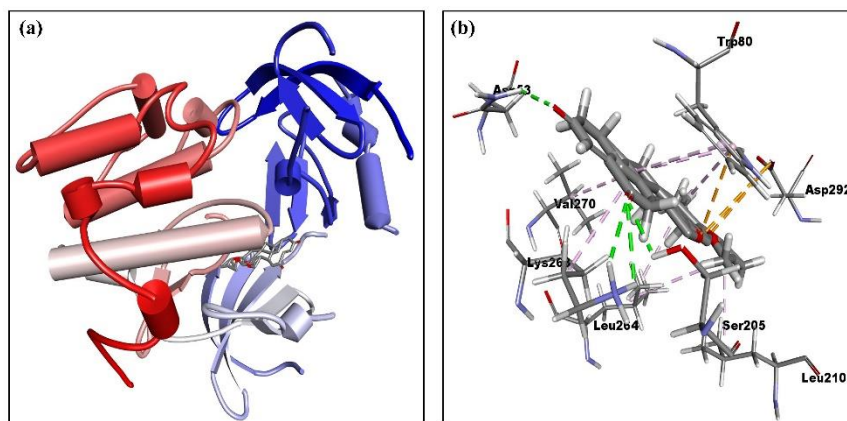


**Figure 2.** (a) Complex structure; (b) 3D interaction of AKT1 with spirostane-3,6-dione.

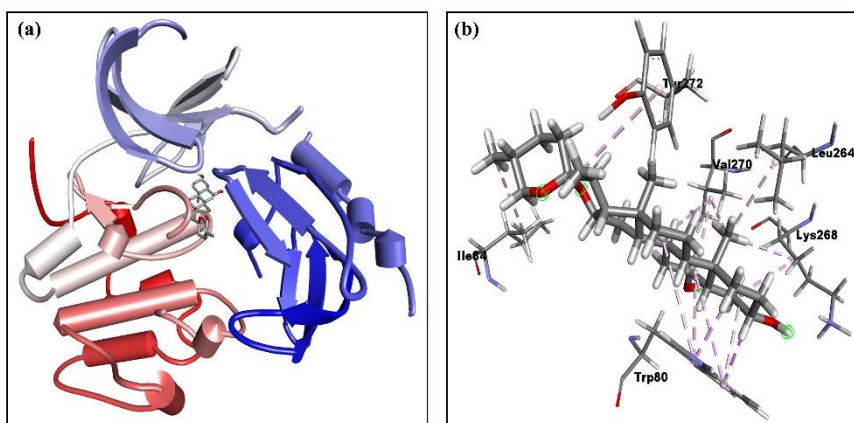


**Figure 3.** (a) Complex structure; (b) 3D interaction of AKT1 with chlorogenicin.

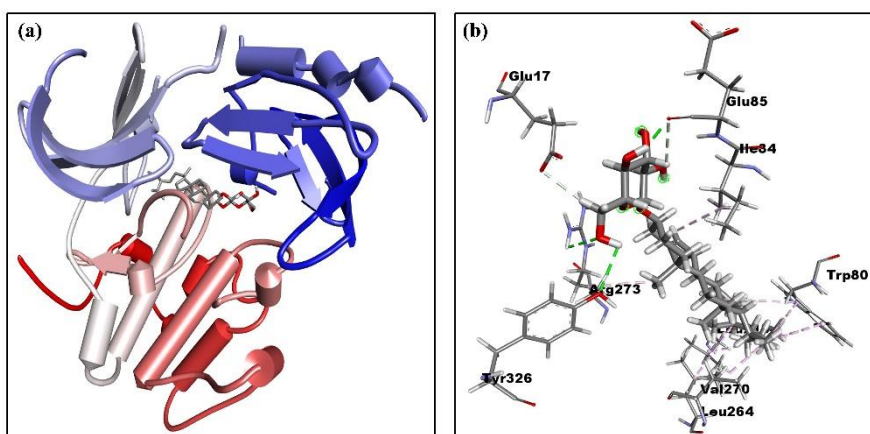


**Figure 4.** (a) Complex structure; (b) 3D interaction of AKT1 with  $\beta$ -sitosterol-d-glucoside.

### 3.5. Physicochemical properties and bioactivity.

The efficacy and metabolic activity of the therapeutic molecules, which are essential for the drug development process, were evaluated using the physicochemical qualities of the molecules. To predict physicochemical properties, a web server named Swiss ADME was employed. Table 3 represents the predicted physicochemical parameters of the top-hit compounds. The effects of orally administered bioactive compounds inside the body should be assessed using the Lipinski rule of five, which states that the molecular weight should be less than 500, hydrogen bond donors should be within 5, hydrogen bond acceptors should be within 10, molar refractivity should be between 40 and 130, and MLOGP should be within 4.15, as

shown in Table 3. Spirostane-3,6-dione, the top binding phytochemical, does not violate the Lipinski rules. Still, chlorogenin and  $\beta$ -sitosterol-d-glucoside from *S. torvum* both have one infraction: chlorogenin for MLOGP > 4.15 and  $\beta$ -sitosterol-d-glucoside for molecular weight >500 [37].

For oral medication distribution, a single infraction is not a big deal. Since the top three binding phytochemicals stated above completely satisfy most of all five requirements, according to the Swiss ADME prediction, they can be utilized as oral medication. The Muegge rules state that a drug's molecular weight (g/mol) should fall between 200 and 600, that XLOGP should be between -2 and 5, that TPSA ( $\text{\AA}^2$ ) should be between 150 and 150, that rings should be between 7 and 8, that heteroatoms should have more than one atom and more than four carbon atoms, that rotatable bonds should be between 10 and 15, and that hydrogen acceptors and donors should be between 10 and 5. The top binding phytochemical, spirostane-3,6-dione, meets the Muegge criterion flawlessly and has no violations according to the aforementioned criteria. The Muegge criteria are mostly met by chlorogenin and  $\beta$ -sitosterol-d-glucoside. However, they do have one violation of XLOGP > 5 [38]. The following two key principles, Veber and Egan, are likewise met by the top three binding phytochemicals [39]. The key phytochemicals, spirostane-3,6-dione, and chlorogenin, satisfy most of Ghose's requirements with just one infraction totaling more than 70 atoms, which is not a major problem. Four of Ghose's conditions are broken by  $\beta$ -sitosterol-d-glucoside: MW>480, WLOGP>5.6, a molar refractivity of >130, and more than 70 atoms [40]. The top three binding phytochemicals best match the drug-like qualities for the innovative drug design, as determined by the physicochemical parameters.

Using the online cheminformatics tool Molinspiration, the top-hit phytochemicals of *Solanum torvum* with breast cancer-associated AKT1 protein were predicted for their bioactivity. Using advanced Bayesian statistics, the Molinspiration prediction showed the following parameters: protease inhibitor, nuclear receptor, ion channel modulator, kinase inhibitor, enzyme inhibitor, and GPCR ligand score [41]. A drug molecule is considered active if its bioactivity score is greater than 0.00, moderately active between -0.50 and 0.00, and inert if it is lower than -0.50. Spirostane-3,6-dione, chlorogenin, and  $\beta$ -sitosterol-d-glucoside all show outstanding enzyme inhibitory activity based on the Molinspiration predictions, with scores of 0.48, 0.65, and 0.41, respectively. With scores of 0.43, 0.61, and 0.33, respectively, the three lead compounds function admirably as nuclear receptor ligands. Spirostane-3,6-dione and chlorogenin perform outstanding dual roles as GPCR ligands and protease inhibitors. With scores of -0.00 and 0.15, spirostane-3,6-dione and chlorogenin perform outstanding ion channel modulation, whereas  $\beta$ -sitosterol-d-glucoside performs modestly. Spirostane-3,6-dione does not function as a kinase inhibitor, although chlorogenin and  $\beta$ -sitosterol-d-glucoside are moderately bioactive as kinase inhibitors with scores of -0.37 and -0.47, respectively. The top-hit phytochemicals of *S. torvum* demonstrate outstanding bioactivity, as predicted by Molinspiration.

**Table 3.** Assessed physicochemical parameters of the lead compounds of *S. torvum*.

Descriptors	Spirostane-3,6-dione	Chlorogenin	$\beta$ -sitosterol-d-glucoside
Formula	C27H40O4	C27H44O4	C35H60O6
Molecular weight (g/mol)	428.60	432.64	576.85
Number of heavy atoms	31	31	41
Number of aromatic heavy atoms	0	0	0
Fraction Csp3	0.93	1.00	0.94
Number of rotatable bonds	0	0	9
Number of H-bond acceptors	4	4	6

Descriptors	Spirostane-3,6-dione	Chlorogenin	$\beta$ -sitosterol-d-glucoside
Number of H-bond donors	0	2	4
Molar Refractivity	121.31	123.23	165.61
TPSA ( $\text{\AA}^2$ )	52.60	58.92	99.38
Log $P_{o/w}$ (iLOGP)	3.81	4.14	4.98
Log $P_{o/w}$ (XLOGP3)	4.45	5.15	7.74
Log $P_{o/w}$ (WLOGP)	5.18	4.76	5.85
Log $P_{o/w}$ (MLOGP)	3.98	4.23	3.96
Log $P_{o/w}$ (SILICOS-IT)	4.58	3.40	5.02
Consensus (Log $P_{o/w}$ )	4.40	4.34	5.51
Bioavailability score	0.55	0.55	0.55

### 3.6. Pharmacokinetic characteristics.

The therapeutic molecule's ADMET (absorption, distribution, metabolism, excretion, and toxicity) properties are crucial in the drug development process. Existing pharmacokinetic and toxicological evaluation processes could be expensive and time-consuming; *in silico* analysis was used to solve this problem [42]. The top three lead phytochemicals of *S. torvum* with AKT1 were predicted using the online web tool pkCSM, and the lead compounds' ADMET properties are displayed in Table 4. Molecules of medications and nutrients must be absorbed through the human digestive tract. Intestinal absorption capacity is the primary requirement for oral medicine molecule and digestive enzyme absorption. Spirostane-3,6-dione, chlorogenin, and  $\beta$ -sitosterol-d-glucoside are the three lead compounds, and the pkCSM prediction states that they all exhibit extraordinary human intestinal absorbance, with percentage levels of 99.602, 96.823, and 79.677. Skin permeability is important for applied topical treatments; if log  $k_p$  is more than -2.5, it is considered to have low skin permeability. The top three lead compounds, spirostane-3,6-dione, chlorogenin, and  $\beta$ -sitosterol-d-glucoside had exceptional skin permeability, with log  $k_p$  values of -3.399, -3.999, and -2.748, respectively, according to the projection. The pkCSM server employed Caco-2 cells as an *in vitro* model to calculate how well oral medications are absorbed. If the predicted log Papp 10<sup>-6</sup> cm/s value was more than 0.90, the permeability to Caco-2 was considered to be strong. With log Papp 10<sup>-6</sup> cm/s values of 1.479 for spirostane-3,6-dione and 1.263 for chlorogenin, respectively, both have good Caco-2 permeability, whereas  $\beta$ -sitosterol-d-glucoside has a somewhat lower log Papp 10<sup>-6</sup> cm/s value of 0.472. The blood-brain barrier (BBB) permeability, central nervous system (CNS) permeability, and steady-state volume of distribution (VD<sub>ss</sub>) were important considerations for evaluating the distribution characteristics of the therapeutic compounds. The recommended dosage must be administered consistently to maintain the drug's concentration at the same level as it does in plasma. Spirostane-3,6-dione and chlorogenin have intermediate volumes of distribution, with log VD<sub>ss</sub> values of 0.19 and 0.192, respectively, according to the pkCSM prediction; however,  $\beta$ -sitosterol-d-glucoside has a somewhat low volume of distribution, with a log VD<sub>ss</sub> of -1.163 log L/kg. With log BB values of -0.05 and 0.004, spirostane-3,6-dione and chlorogenin partly passed the blood-brain barrier, while  $\beta$ -sitosterol-d-glucoside was unable to do so. With logPS values of -1.398 and -1.592, the central nervous system has been partially penetrated by spirostane-3,6-dione and chlorogenin, but not by  $\beta$ -sitosterol-d-glucoside. As shown in Figure 5, the Swiss ADME web tool created a BOILED Egg model using the top three phytochemicals. Spirostane-3,6-dione and chlorogenin were placed slightly inside the yolk region of the model, confirming the molecule's BBB permeability range, while  $\beta$ -sitosterol-d-glucoside was placed slightly near the white region. CYP1A2, CYP3A4, CYP2C9, CYP2C19, CYP2D6, and CYP2E1 are among the several isoforms of the important detoxifying enzyme cytochrome

P450 that the pharmaceutical molecule should not block. The two most important isoforms for drug metabolism are CYP2D6 and CYP3A4. The pkCSM prediction shows that, with the exception of the CYP3A4 substrate mechanism, none of the three lead phytochemicals act as both substrates and inhibitors of other cytochrome P450 isoforms, demonstrating that the lead compounds won't have any negative effects on metabolism. The removal of the medicine from the body after metabolism is crucial; the activation or inhibition of the P-glycoprotein (P-gp), which is present in most excretory organs, was used to confirm drug clearance. The prediction states that only spirostane-3,6-dione functions as a P-gp substrate, whereas the other two top-hit phytochemicals do not work as both P-gp I/II inhibitors and P-gp substrates. The lead phytochemicals spirostane-3,6-dione, chlorogenin, and  $\beta$ -sitosterol-d-glucoside have overall clearance values (log ml/min/kg) of 0.232, 0.346, and 0.689, respectively, indicating that they won't have any negative effects. The medication development procedure required careful consideration of the therapeutic molecule's toxicity. The pkCSM prediction shows that the lead phytochemicals of *S. torvum* do not cause AMES toxicity, proving that they are not carcinogenic. The maximum tolerable dose for humans is good for the three lead phytochemicals. Spirostane-3,6-dione, chlorogenin, and  $\beta$ -sitosterol-d-glucoside had projected rat oral LD50 values of 1.991, 1.976, and 2.271, respectively. Spirostane-3,6-dione, chlorogenin, and  $\beta$ -sitosterol-d-glucoside each had an oral rat chronic toxicity (LOAEL) (log mg/kg bw/day) of 1.211, 1.29, and 3.293, respectively. Spirostane-3,6-dione inhibits hERG II, but other lead compounds do not inhibit hERG I or II. Three top-hit compounds do not result in both hepatotoxicity and skin hypersensitivity, according to the pkCSM prediction [43].

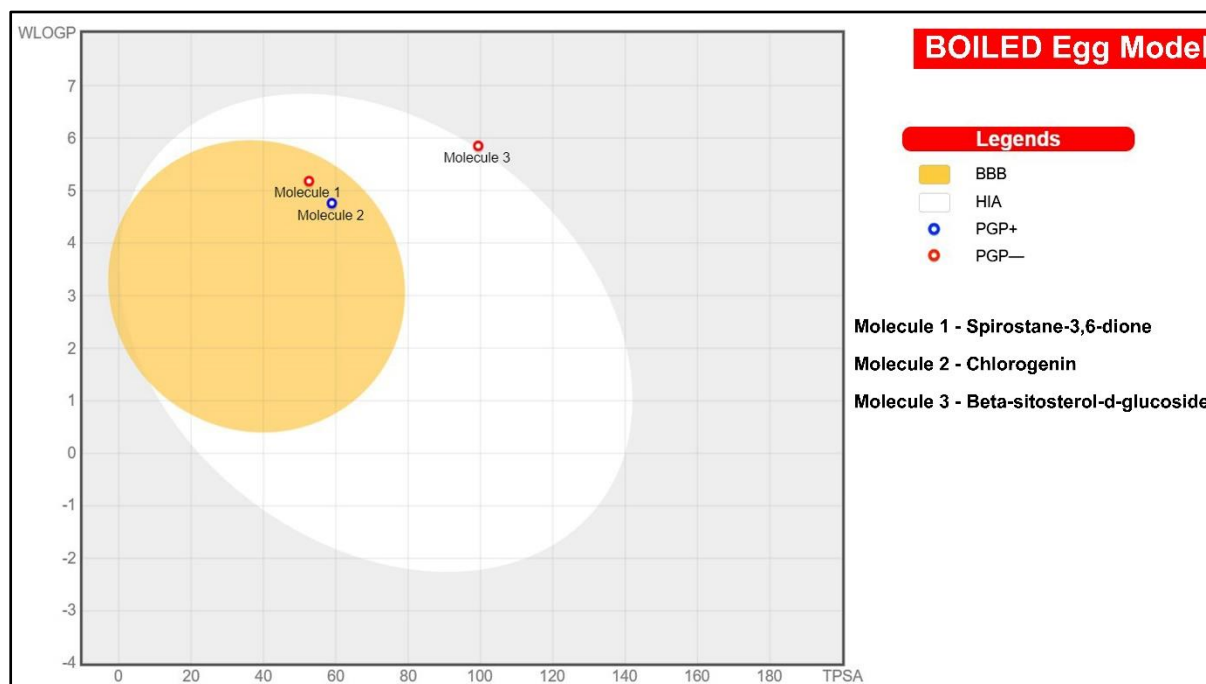


**Figure 5.** Predicted BOILED-Egg model of top hit compounds of *S. torvum*.

**Table 4.** Pharmacokinetic characteristics of the top three lead compounds of *S. torvum*

Descriptors	Spirostane-3,6-dione	Chlorogenin	$\beta$ -sitosterol-d-glucoside
Water solubility (log mol/L)	-5.154	-5.213	-4.741
Caco2 permeability (log Papp in 10 <sup>-6</sup> cm/s)	1.479	1.263	0.472
Human intestinal absorption (% Absorbed)	99.602	96.823	79.677
Skin Permeability (log Kp)	-3.399	-3.999	-2.748
P-glycoprotein substrate	No	Yes	Yes
P-glycoprotein I/II inhibitor	Yes	Yes	Yes
VDss (human) (log L/kg)	0.19	0.192	-1.163

Descriptors	Spirostane-3,6-dione	Chlorogenin	$\beta$ -sitosterol-d-glucoside
BBB permeability (log BB)	0.05	0.004	-0.785
CNS permeability (log PS)	-1.398	-1.592	-3.021
CYP2D6 substrate	No	No	No
CYP3A4 substrate	Yes	Yes	Yes
CYP1A2 inhibitor	No	No	No
CYP2C19 inhibitor	No	No	No
CYP2C9 inhibitor	No	No	No
CYP2D6 inhibitor	No	No	No
CYP3A4 inhibitor	No	No	No
Total Clearance (log mg/kg/day)	0.232	0.346	0.689
Renal OCT2 substrate	Yes	Yes	No
AMES toxicity	No	No	No
Max. tolerated dose (human) (logmg/kg/day)	-0.435	-0.678	-0.887
hERG I inhibitor	No	No	No
hERG II inhibitor	Yes	No	No
Oral Rat Acute Toxicity (LD50)	1.991	1.976	2.271
Oral Rat Chronic Toxicity (LOAEL)	1.211	1.29	3.293
Hepatotoxicity	No	No	No
Skin sensitization	No	No	No

### 3.7. Frontier Molecular orbitals (FMO).

The density functional theory was performed for the top-hit phytochemicals spirostane-3,6-dione, chlorogenin, and beta-sitosterol-d-glucoside from *S. torvum*. The frontier molecular orbitals were computed through density functional theory with B3LYP in a 6-311G basis set using the Gaussian program. The orbitals of LUMO and HOMO were visualized through GaussView software. The frontier molecular orbitals (FMO), also known as the highest occupied (HOMO) and lowest unoccupied (LUMO) molecular orbitals, are the most important orbitals in a molecule. These orbitals determine the relationships between the molecules, which are fundamental in modern biochemistry and molecular biology [44]. The properties of bioactive compounds and their relationships to biological targets are revealed through FMO analysis. The HOMO-LUMO gap explains the molecule's kinetic stability and chemical reactivity, which are essential in determining its electronic properties [45]. Due to its high chemical reactivity and low kinetic stability, a molecule with a narrower gap between LUMO and HOMO is known as a soft molecule. Figures 6-8 depict the molecule's FMOs, and Table 5 lists the relevant molecular characteristics such as LUMO, HOMO, and energy gap values using Koopman's theorem. While the HOMO orbital predominantly serves as an electron donor, the LUMO orbital mostly serves as an electron acceptor. The positive and negative phases are denoted by red and green, respectively. According to the wave function, a single electron is excited from the highest occupied molecular orbital to the lowest unoccupied molecular orbital. This indicates that electron absorption is the transition from the ground state to the first excited state [46]. The energy difference between LUMO and HOMO explains the charge transfer interaction within the molecule. The HOMO electrons are simpler to describe when the energy gap between the LUMO and the HOMO is less. When its energy is high, HOMO finds it easier to donate electrons; yet, when its energy is low, LUMO finds it easier to acquire electrons. The calculated LUMO and HOMO values of spirostane-3,6-dione were -0.5420 eV and -6.1432 eV; for chlorogenin it was calculated to be 2.3404 eV and -6.5215 eV, and for beta-sitosterol-d-glucoside, it was -0.8482 eV and -6.2325 eV, respectively. From the LUMO and HOMO values, the band energy gap was calculated for spirostane-3,6-dione, chlorogenin, and beta-sitosterol-d-glucoside and the calculated values were 5.6012 eV, 8.8619 eV, and 5.3843 eV, respectively.

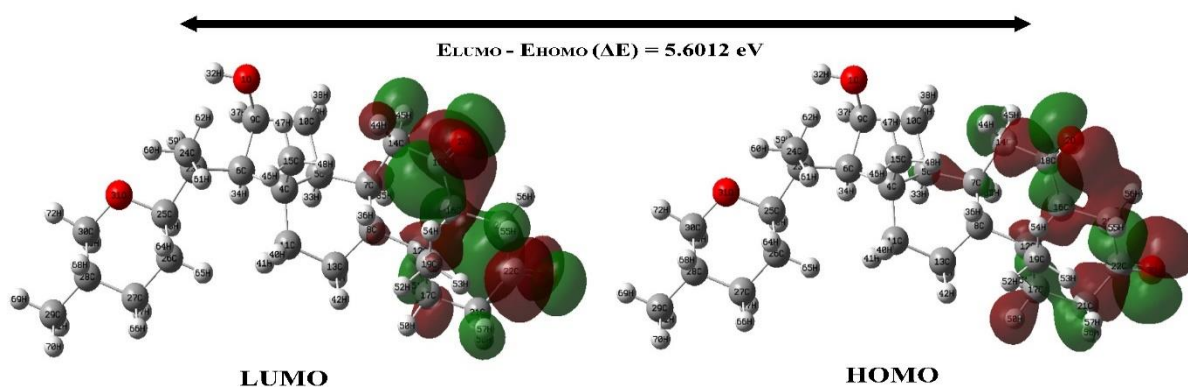


**Figure 6.** The molecular orbitals (LUMO and HOMO) of spirostane-3,6-dione.

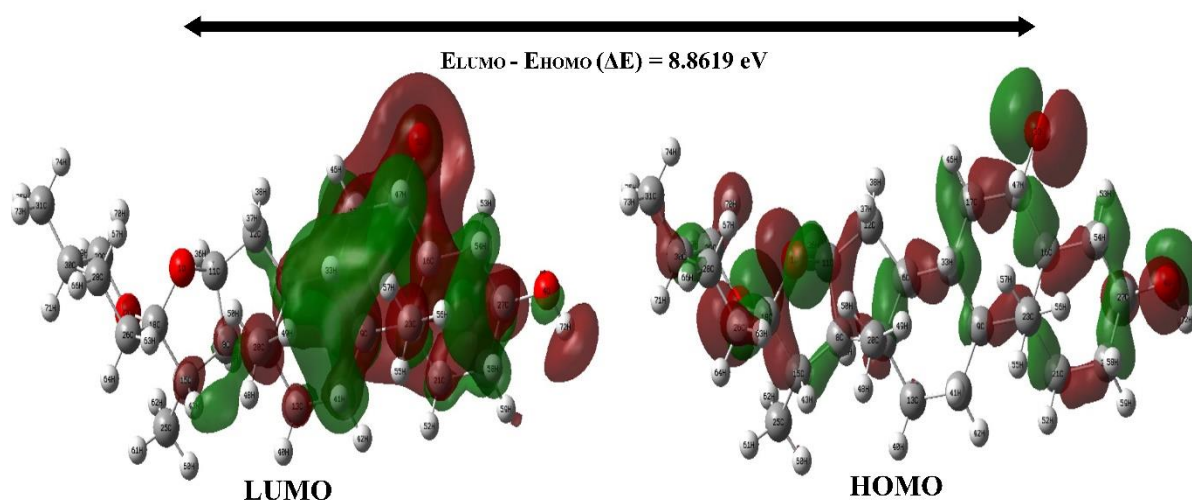


**Figure 7.** The molecular orbitals (LUMO and HOMO) of chlorogenin.

The electron affinity (A) and ionization potential (I), respectively, were the negative energies of LUMO and HOMO,  $A = -ELUMO$  and  $I = -EHOMO$ . The formula  $\chi = (I+A)/2$  was used to calculate the electronegativity ( $\chi$ ) of the molecule, and the negative value of electronegativity ( $\chi$ ) indicates the chemical potential ( $\mu$ );  $\mu = -\chi$  and the chemical hardness ( $\eta$ ) was projected by the formula  $\eta = (I-A)/2$ . The inverse of chemical hardness ( $\eta$ ) denotes chemical softness (S);  $S = 1/\eta$ . For calculating the electrophilicity index ( $\omega$ ), the formula  $\omega = \mu^2/2\eta$  was applied, and nucleophilicity (N) was calculated as the inverse value of electrophilicity;  $N = 1/\omega$ . The values of the top hit compounds spirostane-3,6-dione, chlorogenin, and beta-sitosterol-d-glucoside are shown in Table 5, along with their values for electron affinity, chemical softness, ionization potential, chemical potential, chemical hardness, nucleophilicity, and electrophilicity index. The highest energy gap of 8.8619 eV was attained for the bioactive compound chlorogenin. The chemical reactivity of a molecule is good when the energy gap is low, and the structural stability is good when the energy gap is high. The compounds with moderate energy values of 3 eV to 6 eV possess decent chemical reactivity and structural stability. The higher energy gap in chlorogenin shows lesser chemical reactivity and good structural stability. In spirostane-3,6-dione and beta-sitosterol-d-glucoside, the energy value confirms its higher chemical reactivity and better structural stability.

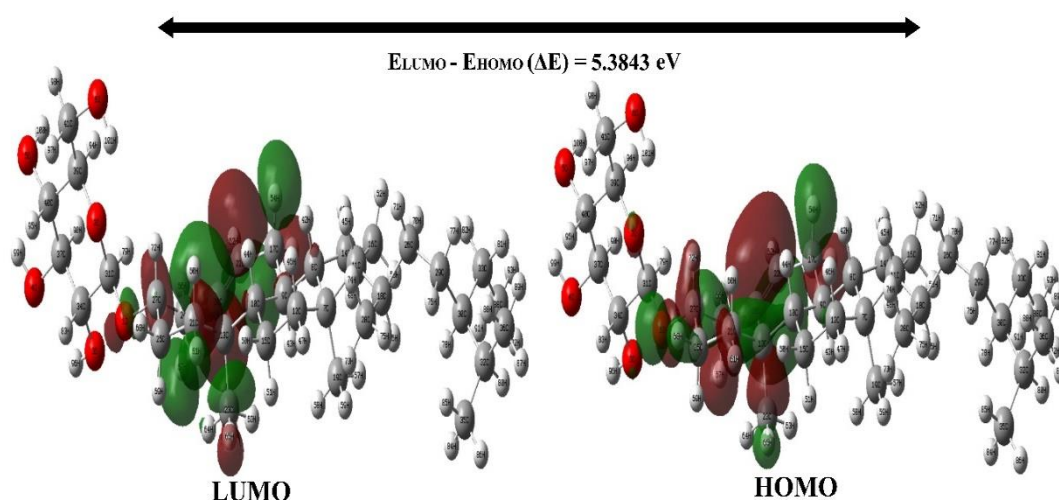


**Figure 8.** The molecular orbitals (LUMO and HOMO) of beta-sitosterol-d-glucoside.

**Table 5.** Calculated molecular characteristics of top hit compounds-based frontier orbitals.

Parameters (eV)	Spirostane-3,6-dione	Chlorogenin	Beta-sitosterol-d-glucoside
$E_{LUMO}$	-0.5420	2.3404	-0.8482
$E_{HOMO}$	-6.1432	-6.5215	-6.2325
$\Delta E (E_{LUMO} - E_{HOMO})$	5.6012	8.8619	5.3843
Electron Affinity (A)	0.5420	-2.3404	0.8482
Ionization Potential (I)	6.1432	6.5215	6.2325
Electronegativity ( $\chi$ )	3.3426	2.0904	3.5404
Chemical Potential ( $\mu$ )	-3.3426	-2.0904	-3.5404
Chemical Hardness ( $\eta$ )	2.8006	4.4309	2.6922
Chemical softness (S)	0.3571	0.2257	0.3714
Electrophilicity Index ( $\omega$ )	1.9948	0.4931	2.3280
Nucleophilicity (N)	0.5013	2.0280	0.4296

### 3.8. Electronic spectrum.

Investigating UV-visible spectra is a practical way to learn more about the electronic states of molecules [47]. In the gaseous phase, the electronic absorption spectra of top-hit compounds spirostane-3,6-dione, chlorogenin, and beta-sitosterol-d-glucoside were calculated using the TD-DFT technique, and the CAM-B3LYP/6-311 G basis set. The excitation wavelength, oscillator strength, wavelength, orbitals, and their contributions were evaluated through an electronic spectrum. Figures 9-11 display spirostane-3,6-dione, chlorogenin, and beta-sitosterol-d-glucoside simulated UV-Visible spectrum graph through TD-DFT.

Three peaks were observed for spirostane-3,6-dione at 243 nm, 311 nm, and 318 nm. The peak 243 nm has an excitation energy of 41105.52  $\text{cm}^{-1}$ , oscillatory strength of 0.0002, and contributions H $\rightarrow$ L (86%) and H-1 $\rightarrow$ L (9%). The peak 311 nm possesses 32152.71  $\text{cm}^{-1}$  excitation energy, 0.0002 oscillator strength, and contributions H-3 $\rightarrow$ L (49%), H-1 $\rightarrow$ L+1 (31%), H-3 $\rightarrow$ L+1 (3%), H-1 $\rightarrow$ L (6%) and H $\rightarrow$ L+1 (4%) and the peak 318 nm exhibits 31437.29  $\text{cm}^{-1}$  energy of excitation, 0.0001 oscillator strength and H-3 $\rightarrow$ L+1 (22%), H-1 $\rightarrow$ L (55%), H-3 $\rightarrow$ L (5%), H-2 $\rightarrow$ L (3%), H-1 $\rightarrow$ L+1 (4%) and H $\rightarrow$ L (8%) contributions. For spirostane-3,6-dione, the transition was assigned to be  $\pi \rightarrow \pi^*$  transition.

The electronic spectrum of chlorogenin exhibited two peaks at 153 nm and 162 nm. The major peak 153 nm possesses excitation energy of 65359.59  $\text{cm}^{-1}$ , 0.0122 oscillator strength and contributions H-3 $\rightarrow$ L+1 (13%), H-1 $\rightarrow$ L+1 (10%), H $\rightarrow$ L+1 (44%), H-3 $\rightarrow$ L (2%), H-2 $\rightarrow$ L+1 (9%), H-2 $\rightarrow$ L+3 (4%) and H $\rightarrow$ L (6%) and the minor peak 162 nm holds excitation energy of 61640.54  $\text{cm}^{-1}$ , oscillator strength of 0.0026 and orbital contributions of H-1 $\rightarrow$ L

(18%), H-1→L+2 (29%), H-1→L+5 (16%), H→L+2 (11%), H-1→L+3 (4%), H→L (8%) and H→L+5 (5%). The designation transition for chlorogenin was  $\sigma \rightarrow \sigma^*$ .

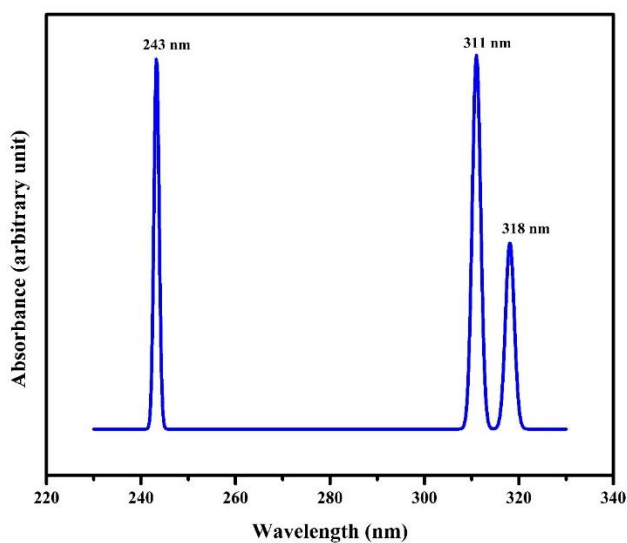


**Figure 9.** The simulated electronic spectrum of spirostane-3,6-dione using TD-DFT.

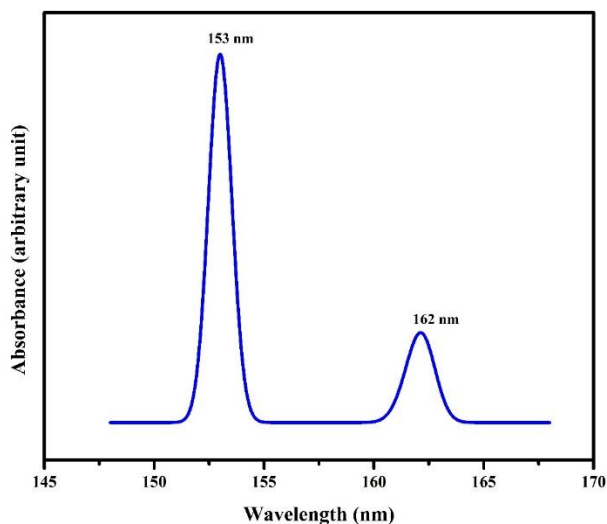


**Figure 10.** The simulated electronic spectrum of chlorogenin using TD-DFT.

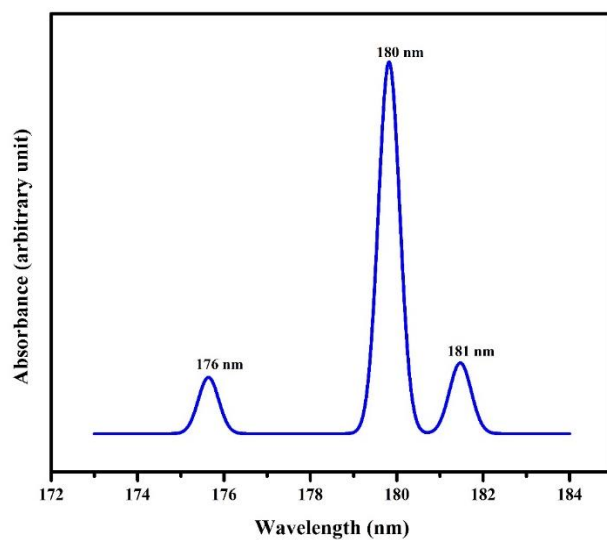


**Figure 11.** The simulated electronic spectrum of beta-sitosterol-d-glucoside using TD-DFT.

One major peak and two minor peaks were observed for phytochemical beta-sitosterol-d-glucoside. The major peak was at 180 nm, and the minor peaks were at 176 nm and 181 nm. The higher peak 180 nm has excitation energy of 55611.51 cm<sup>-1</sup>, oscillatory strength of 0.2004 and orbital contributions of H-5→L (13%), H-1→L (16%), H→L (54%), H-4→L (5%) and H-2→L (9%) and the peak 176 nm has 56934.26 cm<sup>-1</sup>, 0.0304 oscillator strength and H-2→L (79%), H-5→L (2%), H-4→L (6%), H-1→L (3%) and H→L (7%) orbital contributions and the peak 181 nm has 55104.99 cm<sup>-1</sup> energy, 0.0382 oscillatory strength and contributions H-1→L (80%), H→L (15%) and H-5→L (2%), respectively. The electronic transition for phytochemical beta-sitosterol-d-glucoside was assigned to be  $\sigma \rightarrow \sigma^*$  transition.

#### 4. Conclusions

According to the study's findings, all of the bioactive phytochemicals from the *Solanum torvum* had the ability to bind to the target protein AKT1, indicating that they may be effective in the treatment of breast cancer. When compared to the known standard drug tamoxifen, the docking results showed that compounds spirostane-3,6-dione, chlorogenin, and beta-sitosterol-d-glucoside had a better affinity with the docking scores of -17.4 Kcal/mol, -12.2 Kcal/mol, and -11.5 Kcal/mol. The interaction of lead compounds, the type of interactions, and the bond distances were analyzed. The physicochemical and ADME prediction demonstrated the drug-like qualities of spirostane-3,6-dione, chlorogenin, and beta-sitosterol-d-glucoside as an oral medication. The toxicity analysis discovered the lead compounds' safety profile and adverse consequences. Frontier molecular orbitals were used to assess the molecular reactivity, kinetic stability, and intramolecular charge transfer of spirostane-3,6-dione, chlorogenin, and beta-sitosterol-d-glucoside. The energy gap between LUMO and HOMO revealed the chemical reactivity and stability of the lead compounds. The electronic spectrum was performed to observe lead compounds' absorbance range, excitation state, energy, and orbital contributions. These density functional theory calculations showed the three bioactive compounds' stability and reactive nature. These computational studies will pave the way for novel drug discovery from traditional plants. To comprehend the activities and efficacy of *Solanum torvum* for the treatment of breast cancer, further *in vivo* and *in vitro* study is required.

#### Funding

This research was funded by a Grant-aid from the Department of Biotechnology (DBT), Ministry of Science and Technology, India [BT/PR44695/NER/95/1880/2021].

#### Acknowledgments

The authors acknowledge Dr. S. Athimoolam, Department of Physics, University College of Engineering, Nagercoil, for helping us utilize the Gaussian 09 Program.

#### Conflicts of Interest

The authors declare no conflict of interest.

## References

1. Darkwah, W. K.; Koomson, D. A.; Miwornunyuie, N.; Nkoom, M.; Pupilampu, J. B. Review: phytochemistry and medicinal properties of *Solanum torvum* fruits. *All Life*, **2020**, *13*, 498-506, <https://doi.org/10.1080/26895293.2020.1817799>.
2. Mehalya, T.; Sundaram, M. M.; Meenakumari, R. A Drug Review On Silethuma Sura Kiyalam With Kanji–A Siddha Herbal Formulation In The Management Of Kabasuram (Acute Bronchitis) In Children. *Int J Trans Res Ind Med*, **2022**, *4*, 19-24, <http://repository-tnmgrmu.ac.in/20976/>.
3. Loganayaki, N.; Siddhuraju, P.; Manian, S. Antioxidant activity of two traditional Indian vegetables: *Solanum nigrum* L. and *Solanum torvum* L. *Food Science and Biotechnology*, **2010**, *19*, 121-127, <https://doi.org/10.1007/s10068-010-0017-y>.
4. Yuan, B.; Lyu, W.; Dinssa, F.; Hoffman, D.; Simon, J. E.; Wu, Q. African nightshades: recent advances on the phytochemistry, nutrition, and toxicity. *African natural plant products, volume III: Discoveries and innovations in chemistry, bioactivity, and applications*, **2020**, 103-137, <https://doi.org/10.1021/bk-2020-1361.ch005>.
5. Nguta, J. M.; Appiah-Opong, R.; Nyarko, A. K.; Yeboah-Manu, D.; Addo, P. G., Otchere, I.; Kissi-Twum, A. Antimycobacterial and cytotoxic activity of selected medicinal plant extracts. *Journal of ethnopharmacology*, **2016**, *182*, 10-15, <https://doi.org/10.1016/j.jep.2016.02.010>.
6. Allugunti, V. R. Breast cancer detection based on thermographic images using machine learning and deep learning algorithms. *International Journal of Engineering in Computer Science*, **2022**, *4*, 49-56.
7. Li, W.; Hou, J. Z.; Niu, J.; Xi, Z. Q.; Ma, C.; Sun, H.; Xie, S. Q. Akt1 inhibition promotes breast cancer metastasis through EGFR-mediated  $\beta$ -catenin nuclear accumulation. *Cell Communication and Signaling*, **2018**, *16*, 1-13, <https://doi.org/10.1186/s12964-018-0295-1>.
8. Millis, S. Z.; Ikeda, S.; Reddy, S.; Gatalica, Z.; Kurzrock, R. Landscape of phosphatidylinositol-3-kinase pathway alterations across 19 784 diverse solid tumors. *JAMA oncology*, **2016**, *2*, 1565-1573, <https://doi.org/10.1001/jamaoncol.2016.0891>.
9. Manning, B. D.; Cantley, L. C. AKT/PKB signaling: navigating downstream. *Cell*, **2007**, *129*, 1261-1274, <https://doi.org/10.1016/j.cell.2007.06.009>.
10. Sporn, M. B.; Liby, K. T. NRF2 and cancer: the good, the bad and the importance of context. *Nature Reviews Cancer*, **2012**, *12*, 564-571, <https://doi.org/10.1038/nrc3278>.
11. Tan, C. C.; Yu, J. T.; Wang, H. F.; Tan, M. S.; Meng, X. F.; Wang, C.; Tan, L. Efficacy and safety of donepezil, galantamine, rivastigmine, and memantine for the treatment of Alzheimer's disease: a systematic review and meta-analysis. *Journal of Alzheimer's Disease*, **2014**, *41*, 615-631, <https://doi.org/10.3233/JAD-132690>.
12. Liu, H.; Radisky, D. C.; Nelson, C. M.; Zhang, H.; Fata, J. E.; Roth, R. A.; Bissell, M. J. Mechanism of Akt1 inhibition of breast cancer cell invasion reveals a protumorigenic role for TSC2. *Proceedings of the National Academy of Sciences*, **2006**, *103*, 4134-4139, <https://doi.org/10.1073/pnas.0511342103>.
13. Ju, X.; Katiyar, S.; Wang, C.; Liu, M.; Jiao, X.; Li, S.; Pestell, R. G. Akt1 governs breast cancer progression in vivo. *Proceedings of the National Academy of Sciences*, **2007**, *104*, 7438-7443, <https://doi.org/10.1073/pnas.0605874104>.
14. Ooms, L. M.; Binge, L. C.; Davies, E. M.; Rahman, P.; Conway, J. R.; Gurung, R.; Mitchell, C. A. The inositol polyphosphate 5-phosphatase PIPP regulates AKT1-dependent breast cancer growth and metastasis. *Cancer cell*, **2015**, *28*, 155-169, <https://doi.org/10.1016/j.ccell.2015.07.003>.
15. Yoeli-Lerner, M.; Yiu, G. K.; Rabinovitz, I.; Erhardt, P.; Jauliac, S.; Toker, A. Akt blocks breast cancer cell motility and invasion through the transcription factor NFAT. *Molecular cell*, **2005**, *20*, 539-550, <https://doi.org/10.1016/j.molcel.2005.10.033>.
16. Viswanathan, T. M.; Chitradevi, K.; Zochedh, A.; Vijayabhaskar, R.; Sukumaran, S.; Kunjiappan, S.; Kathiresan, T. Guanidine–curcumin complex-loaded amine-functionalised hollow mesoporous silica nanoparticles for breast cancer therapy. *Cancers*, **2022**, *14*, 3490, <https://doi.org/10.3390/cancers14143490>.
17. Carpten, J. D.; Faber, A. L.; Horn, C.; Donoho, G. P.; Briggs, S. L.; Robbins, C. M.; Thomas, J. E. A transforming mutation in the pleckstrin homology domain of AKT1 in cancer. *Nature*, **2007**, *448*, 439-444, <https://doi.org/10.1038/nature05933>.
18. Shannon, P.; Markiel, A.; Ozier, O.; Baliga, N. S.; Wang, J. T.; Ramage, D.; Ideker, T. Cytoscape: a software environment for integrated models of biomolecular interaction networks. *Genome research*, **2003**, *13*, 2498-2504, <https://doi.org/10.1101/gr.1239303>.

19. Berman, H. M.; Westbrook, J.; Feng, Z.; Gilliland, G.; Bhat, T. N.; Weissig, H.; Bourne, P. E. The protein data bank. *Nucleic acids research*, **2000**, *28*, 235-242, <https://doi.org/10.1093/nar/28.1.235>.
20. Duke, J.; & MJ, B. Dr. Duke's phytochemical and ethnobotanical databases. USDA. *Agricultural Research Service*, **1994**, <https://phytochem.nal.usda.gov/>.
21. Mohanraj, K.; Karthikeyan, B. S.; Vivek-Ananth, R. P.; Chand, R. B.; Aparna, S. R.; Mangalapandi, P.; Samal, A. IMPPAT: A curated database of Indian Medicinal Plants, Phytochemistry and Therapeutics. *Scientific reports*, **2018**, *8*, 4329, <https://doi.org/10.1038/s41598-018-22631-z>.
22. Kim, S.; Chen, J.; Cheng, T.; Gindulyte, A.; He, J.; He, S.; Bolton, E. E. PubChem in 2021: new data content and improved web interfaces. *Nucleic acids research*, **2021**, *49*, D1388-D1395, <https://doi.org/10.1093/nar/gkaa971>.
23. Tian, W.; Chen, C.; Lei, X.; Zhao, J.; Liang, J. CASTp 3.0: computed atlas of surface topography of proteins. *Nucleic acids research*, **2018**, *46*, W363-W367, <https://doi.org/10.1093/nar/gky473>.
24. Daina, A.; Michielin, O.; Zoete, V. SwissADME: a free web tool to evaluate pharmacokinetics, drug-likeness and medicinal chemistry friendliness of small molecules. *Scientific reports*, **2017**, *7*, 42717, <https://doi.org/10.1038/srep42717>.
25. Tariq, M.; Sirajuddin, M.; Ali, S.; Khalid, N.; Tahir, M. N.; Khan, H.; Ansari, T. M. Pharmacological investigations and Petra/Osiris/Molinspiration (POM) analyses of newly synthesized potentially bioactive organotin (IV) carboxylates. *Journal of Photochemistry and Photobiology B: Biology*, **2016**, *158*, 174-183, <https://doi.org/10.1016/j.jphotobiol.2016.02.028>.
26. Pires, D. E.; Blundell, T. L.; Ascher, D. B. pkCSM: predicting small-molecule pharmacokinetic and toxicity properties using graph-based signatures. *Journal of medicinal chemistry*, **2015**, *58*, 4066-4072, <https://doi.org/10.1021/acs.jmedchem.5b00104>.
27. Frisch, A. gaussian 09W Reference. *Wallingford, USA*, **2009**, *25p*, 470.
28. Dennington, R.; Keith, T.; & Millam, J. GaussView, version 5, **2009**.
29. Jacquemin, D.; Adamo, C. Computational molecular electronic spectroscopy with TD-DFT. *Density-Functional Methods for Excited States*, **2016**, 347-375, [https://doi.org/10.1007/128\\_2015\\_638](https://doi.org/10.1007/128_2015_638).
30. Szklarczyk, D.; Gable, A. L.; Nastou, K. C.; Lyon, D.; Kirsch, R.; Pyysalo, S.; von Mering, C. The STRING database in 2021: customizable protein-protein networks, and functional characterization of user-uploaded gene/measurement sets. *Nucleic acids research*, **2021**, *49*, D605-D612, <https://doi.org/10.1093/nar/gkaa1074>.
31. Zochedh, A.; Priya, M.; Chakaravarthy, C.; Sultan, A. B.; Kathiresan, T. Experimental and Computational Evaluation of Syringic Acid-Structural, Spectroscopic, Biological Activity and Docking Simulation. *Polycyclic Aromatic Compounds*, **2022**, *43*, 1-33, <https://doi.org/10.1080/10406638.2022.2118332>.
32. Zochedh, A.; Priya, M.; Shunmuganarayanan, A.; Sultan, A. B.; Kathiresan, T. Antitumor and antimicrobial effect of syringic acid urea cocrystal: Structural and spectroscopic characterization, DFT calculation and biological evaluation. *Journal of Molecular Structure*, **2023**, *1282*, 135113, <https://doi.org/10.1016/j.molstruc.2023.135113>.
33. Sharmili Banu, K. R.; Mohana Priya, I.; Azar Zochedh, A. S. Identification of novel bioactive compounds from banana fruit (*Musa sapientum*) as antidepressant in pregnant women: molecular docking, physicochemical and ADMET evaluation. *Asian Journal of Biotechnology and Genetic Engineering*, **2022**, *5*, 9-24.
34. Zochedh, A. A.; Bahadur, S. A.; Kathiresan, T. Quantum chemical and molecular docking studies of naringin: a potent anticancer drug. *Journal of Cardiovascular Disease Research*, **2021**, *12*, 1140-8, <https://doi.org/10.1016/j.molstruc.2023.135403>.
35. Zochedh, A.; Chandran, K.; Priya, M.; Sultan, A. B.; Kathiresan, T. DFT Simulation of Berberine Chloride with Spectroscopic Characterization-Biological activity and Molecular Docking against Breast Cancer. *Polycyclic Aromatic Compounds*, **2023**, *43*, 1-25, <https://doi.org/10.1080/10406638.2023.2201457>.
36. Asiamah, I.; Obiri, S. A.; Tamekloe, W.; Armah, F. A.; Borquaye, L. S. Applications of Molecular Docking in Natural Products-Based Drug Discovery. *Scientific African*, **2023**, e01593, <https://doi.org/10.1016/j.sciaf.2023.e01593>.
37. Zochedh, A.; Chandran, K.; Priya, M.; Sultan, A. B.; Kathiresan, T. Molecular simulation of naringin combined with experimental elucidation-Pharmaceutical activity and Molecular docking against Breast cancer. *Journal of Molecular Structure*, **2023**, *1285*, 135403, <https://doi.org/10.1016/j.molstruc.2023.135403>.
38. Ferrari, I. V.; Di Mario, M. Prediction of physico-chemical property/Biological Activity and ADMET (absorption, distribution, mechanism, excretion, and toxicity) parameters of approved HIV Medications. *Int. J. Sci. Res. in Biological Sciences*, **2022**, *9*, <https://sdbindex.com/Documents/index/00000510/00001-80759>.

39. Hassan, S. S. U.; Abbas, S. Q.; Ali, F.; Ishaq, M.; Bano, I.; Hassan, M., ... & Bungau, S. G. A Comprehensive in silico exploration of pharmacological properties, bioactivities, molecular docking, and anticancer potential of vieloplain F from *Xylopia vielana* Targeting B-Raf Kinase. *Molecules*, **2022**, *27*, 917, <https://doi.org/10.3390/molecules27030917>.
40. Priya, M.; Zochedh, A.; Arumugam, K.; Sultan, A. B. Quantum Chemical Investigation, Drug-Likeness and Molecular Docking Studies on Galangin as Alpha-Synuclein Regulator for the Treatment of Parkinson's Disease. *Chemistry Africa*, **2023**, *6*, 287-309, <https://doi.org/10.1007/s42250-022-00508-z>.
41. Zochedh, A.; Priya, M.; Shunmuganarayanan, A.; Thandavarayan, K.; Sultan, A. B. Investigation on structural, spectroscopic, DFT, biological activity and molecular docking simulation of essential oil Gamma-Terpinene. *Journal of Molecular Structure*, **2022**, *1268*, 133651, <https://doi.org/10.1016/j.molstruc.2022.133651>.
42. Chandran, K.; Shane, D. I.; Zochedh, A.; Sultan, A. B.; Kathiresan, T. Docking simulation and ADMET prediction based investigation on the phytochemical constituents of Noni (*Morinda citrifolia*) fruit as a potential anticancer drug. *In Silico Pharmacology*, **2022**, *10*, 14, <https://doi.org/10.1007/s40203-022-00130-4>.
43. Priya, M.; Zochedh, A.; Chandran, K.; Arumugam, K.; Banu, S.; Chakaravathy, C.; Sultan, A. B. Computer-Aided Analysis of Biochanin-A as a Potential Breast Cancer Drug Based on DFT, Molecular Docking, and Pharmacokinetic Studies. *Letters in Applied NanoBioScience*, **2022**, *12*, 165, <https://nanobioletters.com/wp-content/uploads/2022/12/LIANBS124.165.pdf>.
44. Zochedh, A.; Shunmuganarayanan, A.; Sultan, A. B. Conformational fidelity and hydrogen bond associability of L-histidine with sulfamate anion studied through XRD, quantum chemical, spectroscopic and molecular docking simulation as a cdk-4 inhibitor against retinoblastoma. *Journal of Molecular Structure*, **2023**, *1274*, 134402, <https://doi.org/10.1016/j.molstruc.2022.134402>.
45. Novena, L. M.; Athimoolam, S.; Anitha, R.; Bahadur, S. A. Synthesis, crystal structure, hirshfeld surface analysis, spectral and quantum chemical studies of pharmaceutical cocrystals of a bronchodilator drug (Theophylline). *Journal of Molecular Structure*, **2022**, *1249*, 131585, <https://doi.org/10.1016/j.molstruc.2021.131585>.
46. Thangarasu, S.; Siva, V.; Kannan, S.; Bahadur, S. A.; Athimoolam, S. Polymorphism in Chloride Salt of m-Nitroaniline: Structural, Spectroscopic, Thermal, Molecular Docking, Biological, and Quantum Chemical Computational Investigation. *Polycyclic Aromatic Compounds*, **2022**, *43*, 1-18, <https://doi.org/10.1080/10406638.2022.2130374>.
47. Sukumaran, S.; Zochedh, A.; Viswanathan, T. M.; Sultan, A. B.; Kathiresan, T. Theoretical Investigation of 5-Fluorouracil and Tamoxifen Complex–Structural, Spectrum, DFT, ADMET and Docking Simulation. *Polycyclic Aromatic Compounds*, **2023**, *43*, 1-18, <https://doi.org/10.1080/10406638.2022.2164018>.